Modes of Catalytic Regeneration in Diesel Particulate Filters

Grigorios C. Koltsakis and Anastasios M. Stamatelos*

Laboratory of Applied Thermodynamics, Aristotle University Thessaloniki, 540 06 Thessaloniki, Greece

The diesel particulate filter (DPF) technology with the use of fuel additives as regeneration aids is a promising technology for modern and future low-emissions diesel engines. The development of efficient and reliable DPF systems requires understanding of the regeneration process. Although the role of mathematical models in this respect has been widely recognized, few attempts to model the fuel-additive-assisted regeneration have been presented. In this work, a previously developed simplified authors' model is extended, to allow deeper investigation of the process. The 1D mathematical model of the catalytic regeneration in the channel of the particulate filter is based on a dynamic oxygen storage/release mechanism of additive action, coupled to the transport phenomena occurring in the filter. A previously published set of full-scale measurements is employed to validate the model in a wide range of possible regeneration modes. The advantages of the present 1D model over the previous 0D model are illustrated. It is concluded that, at the present stage, the model can sufficiently describe and explain the main features of the regeneration process. The minor deviations of the model results from reality are attributed to the uncertainties of the reaction kinetics and to nonuniformities regarding flow distribution and soot deposition. The possible explanations are discussed, and directions for future work are suggested.

Introduction

Diesel engines of the year 2000 will require advanced integrated exhaust aftertreatment systems in order to meet the substantial reductions in total particulate matter (TPM) and NO_x emissions, mandated by legislation in the United States and the European Union. Diesel particulate filters (DPF's) are a viable solution to achieve a substantial TPM reduction in the foreseeable future (Zelenka et al., 1996). The experience with DPF's hitherto has shown that the main problem yet to be solved is the demonstration of high reliability/durability, analogous to that of the exhaust system (on the order of 300 000 km). This is closely related to the control of periodic filter regeneration by combustion of the deposited soot particles. Frequent filter regeneration prevents undesired backpressure buildup due to the accumulated particles in the filter. Regeneration control should additionally ensure filter protection from overheating from reaction exothermy.

Significant knowledge regarding the operational characteristics of traps and their catalytic regeneration behavior has been acquired over the last 15 years. However, common questions arising in the design and manufacture of DPF systems are usually answered rather empirically. These questions refer to (i) optimum material and geometry of a DPF for a given engine, (ii) optimum positioning of a DPF in the exhaust line, (iii) the effect of DPF on engine backpressure (which affects fuel consumption and maximum attainable torque), (iv) the optimum fuel additive dosimetry for each application case.

The frequency of filter regeneration determines the engine backpressure levels during real world operation, whereas the evolution of filter regeneration is critical for its safety. Obviously, the successful design of DPF systems strongly depends on the theoretical knowledge of the regeneration process. This would allow more efficient control in filter loading and fuel-additive dosimetry, thus assisting the development of simple and reliable systems.

To this end, the role of mathematical models has been widely recognized. Recently, the authors presented a "zero-dimensional" catalytic regeneration model which was validated for certain high-flow rate applications (Koltsakis and Stamatelos, 1996a). In this paper, an extended comprehensive one-dimensional model is presented, capable of predicting axial propagation of the reaction. The model includes transport phenomena through the porous soot deposit and filter layers, a redox mechanism of action of transition-metal fuel additives, and finite selectivity with respect to CO of the carbonaceous soot oxidation reaction.

In real practice, two main categories of filter regeneration may be distinguished: The first one involves high-speed and load engine operation associated with high exhaust temperatures and flow rates. The second category is usually met during idle operation following operation at medium load. It is associated with low flow rates but with sufficiently high filter temperatures due to filter thermal inertia. On-road experience with diesel filters (Pattas et al., 1988, 1990) indicates that (a) without catalytic aids high-flow-rate regeneration is responsible for the major part of soot oxidized and (b) in the case of fuel-additive-assisted filter systems low-flow-rate regeneration prevails, especially during city driving.

Extension of the previous catalytic regeneration model to 1D was motivated by the necessity for enhanced prediction accuracy in the study of low space velocity regeneration.

The reaction kinetics parameters appearing in the model can be tuned to represent the catalytic activity of a variety of fuel additives. In this paper we present the procedure of model validation with a copper-based additive for which there exists a complete published experimental study of the regeneration evolution along the filter (Tan et al., 1996). A Cummins LTA 10-300, 10 L, 6-cylinder, direct-injection (DI), turbocharged, and aftercooled diesel engine (224 kW rated power at 1900 rpm) had been used in these experiments.

* Author to whom correspondence is addressed. Telephone: +30-31-996066. Fax: +30-31-996019. E-mail: tassos@antiopi.meng.auth.gr.

S0888-5885(97)00095-X CCC: $14.00

Fundamentals of Catalytic Regeneration. In the absence of catalytic assistance, complete filter regeneration occurs at temperatures above 550 °C, depending on the exhaust flow rate and oxygen concentration. A critical dimensionless number correlating important parameters affecting the regeneration mode is the following Damkoehler number:

$$Da = \frac{t_{\text{flow}}}{t_{\text{reaction}}} = \frac{W\rho_g y S_p k_1(T_w)}{V_w \rho_p} \quad (1)$$

As discussed in detail in Koltsakis and Stamatelos, 1996b, under a critical *Da* number, no regeneration is observed. Higher *Da* numbers characterize more intense regeneration modes.

Soot ignition at lower temperatures often results in partial combustion of the deposited soot in the filter, leaving behind a less reactive carbonaceous residue. Soot can differ considerably in its reactivity according to the degree of graphitization after partial oxidation and the amount of hydrogen retained.

The use of catalytic fuel additives, based on transition metals such as Mn, Cu, Fe, Ce, and Pb, finely dispersed during the fuel combustion process throughout the soot particles, results in regeneration temperatures as low as 350 °C (Wiedemann et al., 1983; Pattas and Michalopoulou, 1992; Johnson et al., 1994). Stochastic regenerations though may be observed even down to 200 °C under favorable engine and filter operating conditions (Lepperhoff et al., 1995). Minor secondary effects that may arise by the use of catalytic fuel additives include incomplete filter cleaning and filter backpressure increase due to the retaining of fuel-additive ash after regeneration.

Stochastic regeneration behavior observed at low temperatures (Lepperhoff et al., 1995; Wiedemann et al., 1983) probably has its roots in the presence of the volatile hydrocarbon. The volatile fraction originates from unburned fuel and lubricating oil and is found adsorbed/condensed on the soot particles at temperatures below 200 °C. In this case, the regeneration initiates in specific channels of the monolith, where the local soot loading and temperatures are favorable. The associated heat release, apart from the soot, gasifies and ignites the volatile hydrocarbons, thus enhancing the propagation of the reaction. These, unpredictable, low-temperature regenerations may also be "ignited" by hot particles originating from engine deposits formed by the additive (Lepperhoff et al., 1995).

Several mechanisms have been suggested to expain the catalytic activity of metal compounds on carbon/soot oxidation/combustion (McKee, 1981). Due to the strong oxygen concentration dependence of the action of transition-metal oxides, a redox mechanism is usually invoked to explain their catalytic activity (Cotton et al., 1971; Ahlstroem and Odenbrand, 1990; Yuan et al., 1994): the additive stores and exchanges oxygen atoms with the surrounding carbonaceous matrix and gas. However, additional mechanisms involving catalyzed thermal decomposition of water vapor and soot oxidation by hydroxyl radicals (Cotton et al., 1971), or electron exchange among additive and carbon atoms resulting in a weakening of the carbon bonds in the boundaries of the carbon matrix facilitating thus reaction with oxygen, have also been proposed.

The above-mentioned mechanisms are not as efficient when catalytic coatings are applied on wall-flow filters, due to poor microscale contact among the carbonaceous particle matrix and the catalyst active sites. This explains why coatings have not proven as effective as fuel additives. Even under favorable conditions, less than 100 °C decrease in ignition temperatures is attained (McCabe and Sinkevitch, 1987).

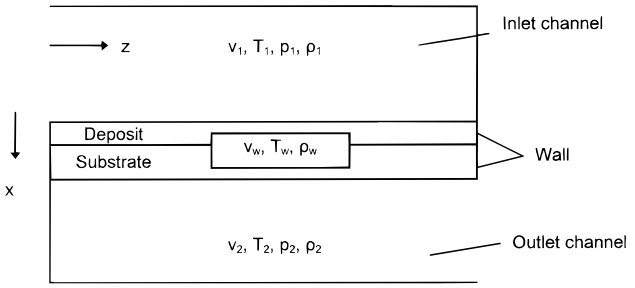

Figure 1. Schematic diagram of single inlet and outlet channels with the substrate wall and the soot deposit layer.

Mathematical Model

Mathematical models of the regeneration process without catalytic aids have been developed to understand the phenomenon and optimize filter systems since the early 1980s (Bissett and Shadman, 1983). Some attempts to explain fuel-additive activity through phenomenological modifications of the kinetics of soot combustion in noncatalytic (thermal) regeneration models have been presented (Hoffmann and Ma, 1989; Hoffmann et al., 1991). It is believed, however, that catalytic regeneration models should rely on a valid theory for fuel-additive action.

There exist two major hypotheses for the catalytic activity of fuel additives (McKee, 1981): the electron-transport theory and the oxygen-transport theory. According to the first theory, electron exchange among additive and carbon atoms results in a weakening of the carbon bonds in the boundaries of the carbon matrix, which enhances reaction with oxygen. According to the second theory, the additive chemically stores and exchanges oxygen atoms with the surrounding carbon and exhaust gas.

Based on the second approach, a zero-dimensional mathematical model has been previously formulated and presented by the authors (Koltsakis and Stamatelos, 1996a). Zero-dimensional models assume flow conditions identical with those of the exhaust gas flowing through the filter wall along the channel. This assumption is quite realistic for high-flow rate operation. However, operation with low flow rates is interesting especially during regeneration with the engine idling, which is a possible filter failure scenario. In the latter case, significant variations in flow and temperature conditions are expected along the channel, which should be predicted by an extended 1D model. The development of this model, which is the main subject of this work, is presented below:

Figure 1 presents a schematic diagram of the monolith inlet and outlet channels with the substrate wall and the soot deposit layer. The exhaust gas temperatures, densities, velocities, and pressures are always expressed as radially averaged values. Previous work (Bisset and Shadman, 1983) has shown that conduction in the thin *x*-direction in the ceramic filter phase is so dominant that the wall temperature may be taken to be independent of *x*, even though the heat from the reaction is only produced in the deposit layer. The interphase heat transfer within the wall is so large that

the gas and solid temperatures may be taken to be equal except in a very thin boundary layer at the interface with the inlet channel. The governing equations for the conservation of mass, momentum, and energy in the flowing exhaust gas are given below:

Conservation of Mass of Channel Gas. In the balance equation for mass conservation, the mass flowing into or from the elementary control volume through the filter wall should be taken into account:

$$\frac{\partial}{\partial z}(\rho_i v_i) = (-1)^i (4/D)\rho_w v_w \tag{2}$$

Conservation of *z*-Component of Momentum of Channel Gas.

$$\frac{\partial p_i}{\partial z}(\rho_i {v_i}^2) = -\alpha_1 \mu v_i / D^2 \tag{3}$$

The right-hand-side term of eq 3 represents the pressure losses in the axial flow direction z caused by the viscous drag forces. Since the mass flow passing through the wall is only a small fraction of the axial flow, the velocity profile should be close to that observed in flows in closed channels. Thus, the relation used to compute the pressure loss is the one used for laminar flows in square ducts.

Conservation of Energy of Channel Gas. In the formulation of the energy balance of the channel gas, we take into account the convective heat exchange with the channel wall, as well as the enthalpy flowing into or from the elementary control volume through the filter wall. For the inlet channel the gas leaves the control volume at temperature T_1:

$$C_{pg}[D^2\rho_1 v_1 T_1|_{z+\Delta z} - D^2\rho_1 v_1 T_1|_z + 4D\Delta z \rho_w v_w T_1|_z] = h_1[4D\Delta z(T_w - T_1)] \tag{4}$$

Combining eqs 2 and 4, we obtain

$$C_{p,g}(\rho_1 v_1)|_{z+\Delta z}\frac{\partial T}{\partial z} = h_1(4/D)(T_w - T_1) \tag{5}$$

On the other hand, for the outlet channel, the gas enters the control volume at temperature T_w:

$$C_{p,g}[D^2\rho_2 v_2 T_2|_{z+\Delta z} - D^2\rho_2 v_2 T_2|_z - 4D\Delta z \rho_w v_w T_w|_z] = h_2[4D\Delta z(T_w - T_2)] \tag{6}$$

Analogously, combining eqs 2 and 6

$$C_{p,g}(\rho_2 v_2)|_z \frac{\partial T}{\partial z} = (h_2 + C_{p,g}\rho_w v_w)(4/D)(T_w - T_2) \tag{7}$$

Soot Combustion and CO Selectivity. Typical diesel particulates consist mainly of a carbonaceous core (soot formed during combustion), adsorbed compounds such as unburnt and partially oxygenated hydrocarbons, sulfates (due to oxidation of the sulfur contained in the fuel), and metal oxides (Vuk et al., 1976). Related research (Johnson et al., 1994) has shown that CO selectivity of the soot oxidation reaction is finite and weakly affected by temperature to the extent that it can be assumed constant up to 700 °C. However, the presence of water vapor introduces a strong dependence on temperature paralleling the temperature dependence of the water−CO gas shift reaction. The incomplete carbon oxidation is assumed to be described by the following reaction:

$$C + \alpha O_2 \rightarrow 2(\alpha - 0.5)CO_2 + 2(1 - \alpha)CO \tag{8}$$

where α is an index of the completeness of the reaction, taking values from 0.5 to 1. For modeling purposes, the parameter α should, be estimated beforehand by means of exhaust gas analysis. Measured values for soot reported in the literature range between 0.55 and 0.9 (De Soete, 1987; Aoki et al., 1993).

ΔH indicates a combined reaction enthalpy resulting from the complete and incomplete oxidation of carbon, which is linked to α according to the relation:

$$\Delta H = 2(\alpha - 0.5)\Delta H_{(i)} + 2(1 - \alpha)\Delta H_{(ii)} \tag{9}$$

The overall rate of soot combustion without catalytic aids is assumed to follow a simple Arrhenius type expression:

$$k_1 = kT e^{-E/RT} \tag{10}$$

For the apparent activation energy E appearing in eq 10, several values have been proposed ranging from 80 000 to 160 000 J/mol (Pattas and Michalopoulou, 1992; Bissett and Shadman, 1985, Pauli et al., 1984; Hoffmann and Ma, 1990). Engine experiments and theoretical investigations (Lepperhoff and Kroon, 1984; Koltsakis and Stamatelos, 1996b) indicate that a value of 150 000 J/mol satisfactorily represents regeneration reaction behavior. Having adopted a value for the apparent activation energy, the factor has been accordingly tuned to obtain good agreement between calculations and measurements.

Kinetics and Mechanism of Additive Action. The commonly used transition-metal additives for promoting filter regeneration form more than one type of oxides corresponding to the possible valence states they can assume. We can, therefore, distinguish between the metal being in “higher” or “lower” oxidation state. The approach presented here refers to regeneration catalyzed by transition-metal fuel additives, existing as well-dispersed oxides with varying valence states inside the porous soot deposit in the filter. Soot oxidation by the catalyst oxides triggers the ignition of the remaining soot. The fuel additive is present in the combustion process, leaves the combustion chamber, and accumulates in the filter together with the emitted soot. Typical filtration efficiencies for additives in the filter are usually over 95% (e.g., Lepperhoff et al., 1995). We can assume that during this process each metal additive molecule is bonded with a number of soot constituents, such as carbon and hydrocarbon molecules. By reaching the filter, the metal additive is assumed to be in its higher oxidation state. Provided that the filter temperature reaches a sufficiently high value, the metal oxide in the deposit layer releases an oxygen atom to react with soot and assumes its lower oxidation state. The reduced oxides produced in this way may react at the same time with the oxygen contained in the flowing exhaust gas. This continuing oxidation/reduction process, which takes place at significantly lower temperatures than unaided soot oxidation, results in the reaction of soot with oxygen from the exhaust gas via the fuel additive, which acts as a catalyst itself.

The catalyst concentration in the soot layer can be described by the following definition:

$$\xi = \frac{\text{moles of metal oxides present in soot}}{\text{carbon moles present in soot}} \quad (11)$$

The fraction ξ is a function of the metal additive concentration in the fuel as well as the engine soot emissions produced during the filter loading operation. Metal additive oxides can, in principle, be present in the deposit layer in both the lower and the higher oxidation states. We define

$$\psi = \frac{\text{"higher oxidation state" metal oxides present in soot}}{\text{total metal oxides present in soot}} \quad (12)$$

During catalytic regeneration the oxidation state of the metal oxides may be changed by reacting either with oxygen of the exhaust gas or with the carbon atoms of the deposit layer. Thus, if we assume that the metal additive Me forms oxides with its 1- and 2-valent states, the following redox reactions take place:

$$C + 4\alpha_{cat}MeO \rightarrow 2\alpha_{cat}Me_2O + 2(\alpha_{cat} - 0.5)CO_2 + 2(1 - \alpha_{cat}CO) \quad (13)$$

$$Me_2O + {}^1/_2O_2 \rightarrow 2MeO \quad (14)$$

where α_{cat} is here an index for the completeness of the catalytic carbon oxidation, taking values from 0.5 to 1.

These reactions combine with reaction (8) to complete the reaction scheme for catalytic soot oxidation. They represent a continuous oxidation/reduction process of the metal oxides present in the deposit soot layer. The rate of the reduction reaction (13) is assumed to follow an Arrhenius type temperature dependence according to the following equation:

$$R_{red} = k_{red}\psi e^{-E_{red}/RT} \quad (15)$$

The rate of the heterogeneous oxidation reaction (14) is expected to be proportional to the oxygen content of the exhaust gas, as well as to the availability of "lower oxidation state" metal oxides, which is expressed by $1 - \psi$. An Arrhenius type temperature dependence is also assumed here. The reaction rate for (15) is then

$$R_{ox} = k_{ox}[O_2](1 - \psi)e^{-E_{ox}/RT} \quad (16)$$

The total rate of change of ψ may then be written as

$$\frac{d\psi}{dt} = R_{ox} - R_{red} \quad (17)$$

Considering the stoichiometry of the reduction reaction, the mass balance equation for the deposit layer, assuming that the deposit is consumed in a shrinking mode, gives (Koltsakis and Stamatelos, 1996a):

$$\rho_p \frac{dw}{dt} = -\left(\frac{M_c}{M_{O_2}}\right)\rho_w v_w y \frac{1}{\alpha}\left(1 - \exp\left(-\frac{S_p k_1 (T_w) w}{v_w}\alpha\right)\right) - \frac{1}{2\alpha_{cat}}\rho_p w \xi R_{red} \quad (18)$$

Energy Balance in the Wall. The energy balance equation for the wall should take into account the contributions of convective heat transfer from the channel flow and from the flow through the wall, the heat released by the exothermic soot combustion, and the conductive heat transfer along the channel wall:

$$\frac{\partial}{\partial t}(\rho_p C_{p,p} T_w + \rho_s C_{p,s} T_w) = h_1(T_1 - T_w) + h_2(T_2 - T_w) + \rho_w v_w C_{p,g}(T_1 - T_w) + H_{react} + H_{cond} \quad (19)$$

From the equation for the consumption rate of the deposit (18), we can compute the heat released by the overall reaction expressed per unit time and area:

$$H_{react} = \left(-\frac{\Delta H}{M_{O_2}}\right)\rho_w v_w y \frac{1}{\alpha}\left[1 - \exp\left(-\frac{S_p k_1 (T_w)_w}{v_w}\right)\right] - \frac{1}{4\alpha_{cat} M_c}\rho_w v_w \Delta H \xi R_{red} \quad (20)$$

The contribution of heat conduction is

$$H_{cond} = -\lambda_p \frac{\partial}{\partial z}\left(w \frac{\partial T_w}{\partial z}\right) - \lambda_s w_s \frac{\partial^2 T_w}{\partial z^2} \quad (21)$$

Pressure Drop across the Deposit Layer and Ceramic Wall. In order to compute the flow field in the filter channel, a correlation for the pressure drop through the soot layer and the filter wall is needed. The porous ceramic wall and the soot deposit are viewed as two porous media in series and the respective pressure drop is computed using the well-known Darcy's law:

$$p_1 - p_2 = \frac{\mu}{k_p} v_w w + \frac{\mu}{k_s} v_w w_s \quad (22)$$

This approach has been previously extensively validated for typical particulate filter applications (Sorenson et al., 1994; Pattas et al., 1997).

Initial and Boundary Conditions. The initial temperature, soot loading, and catalyst concentration along the channel wall are provided as intial conditions for the model which may be axially nonuniform. The boundary conditions, which need to be defined, include the exhaust gas temperature, flow rate, and oxygen content as functions of time as well as the pressure at the filter exit.

Solution Procedure. The governing equations presented above are solved numerically with finite difference techniques using an iterative procedure in the spatial direction controlled by the requirements of zero axial velocity at the end of the inlet channel and atmospheric pressure at the end of the exit channel. Time marching was effected with a fourth-order Runge–Kutta technique. Specifically, the solution procedure is comprised of the following steps:

(a) Computation of the gas flow quantities (pressure, axial and wall velocity, temperature distribution) in the inlet and outlet channels using an iterative procedure: A value for the pressure at the first node of the exit channel is assumed. An arbitrary value for the pressure at the first step of the inlet channel is assumed, and the wall velocity at the first node is computed by solving eq. 22. With the wall velocity known, numerical integration of eq 2 provides the gas velocities for the next space step. Equation 5 gives the gas temperatures at the next node. Based on the variation of the flow rate in the z-direction and the known relationships for

Table 1. Specifications of the Filter Used in the Experiments and Simulations

filter type	EX-80 (single extrusion)
diameter × length	290 × 360 mm
total filtering area	12.2 m^2
cell density	15.5 channels/cm^2 (100 cpsi)
wall thickness	0.43 mm
porosity	50%
mean pore size	12 μm

pressure drop in laminar flows, the gas pressures at the next node can also be computed by integrating eq 3. The above procedure may be continued along the channel length, and a value for the axial velocity at the last node is determined. If this value is not small enough (less than 0.01 times the velocity of the first node), the initial inlet pressure estimation is corrected and the procedure is repeated from the point of the inlet channel pressure estimation. The second criterion to be satisfied is that the pressure at the last node of the outlet channel should be equal to atmospheric. If this is not the case, a new value for the pressure at the first node of the outlet channel is assumed and the procedure restarts from the beginning. The corrections are done using a secant method, to achieve faster convergence.

(b) With the flow quantities known, eqs 17 and 18 are solved for each node by fourth-order Runge−Kutta techniques to provide the variations in w and ψ. In the same manner, eq 20 gives the heat released by the exothermal soot combustion. The heat balance partial differential equation (19) may then be solved explicitly to get the new temperature profile along the channel wall.

Regeneration at High Space Velocities. A typical regeneration in actual vehicle operating conditions occurs during engine operation at high speed−high load, where the exhaust gas temperature is sufficiently high. In this section we employ the 1D catalytic regeneration model described above to study this mode of regeneration. As mentioned above, all runs refer to regeneration experiments conducted by Tan et al. (1996) with a 10 L, 6-cylinder, DI, turbocharged, and aftercooled engine, equipped with a Corning EX-80 filter. The specifications of the filter used in the experiments and simulations are given in Table 1. A total of 33 ppm of Lubrizol, copper-based fuel additive was used throughout the experiments with high space velocity.

Figure 2 presents the operating conditions assumed in regards to exhaust gas inlet temperature, flow rate, and oxygen content as functions of time. After continuous operation at 25% of maximum load, the load is gradually increased and stabilized at its maximum value.

In the following, two high space velocity regenerations with different initial filter loadings will be examined.

Figure 3a presents the measured temperatures during regeneration of a highly loaded filter (initial particulate loading 155 g) (Tan et al., 1996). Significant variations are observed in the evolution of temperatures measured at three characteristic points along the filter axis. The highest temperatures are recorded near the filter exit, reaching a maximum value of about 560 °C. Figure 3b presents the result of computational prediction for this experimental case. The model shows a remarkable ability in predicting the temporal evolution of temperatures along the filter axis.

An additional feature of the model, which is very useful in the study of regeneration reaction propagation, is demonstrated in Figure 4. This figure shows the computed temporal evolution of axial profiles of the

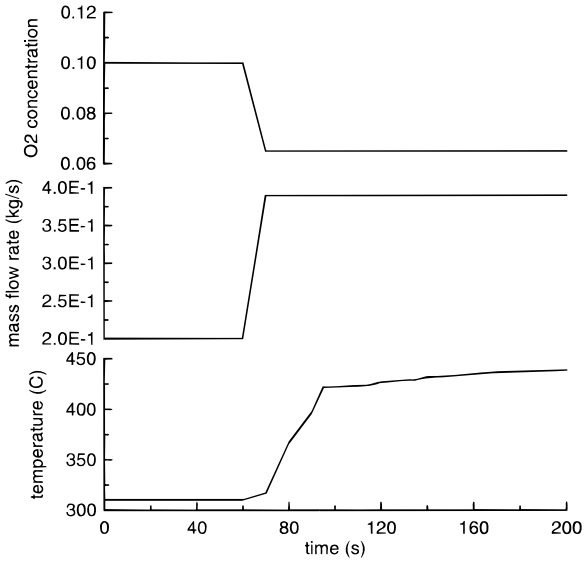

Figure 2. High space velocity regeneration scenario employed in this study. Exhaust gas temperature at filter inlet, exhaust gas flow rate, and oxygen content as functions of time.

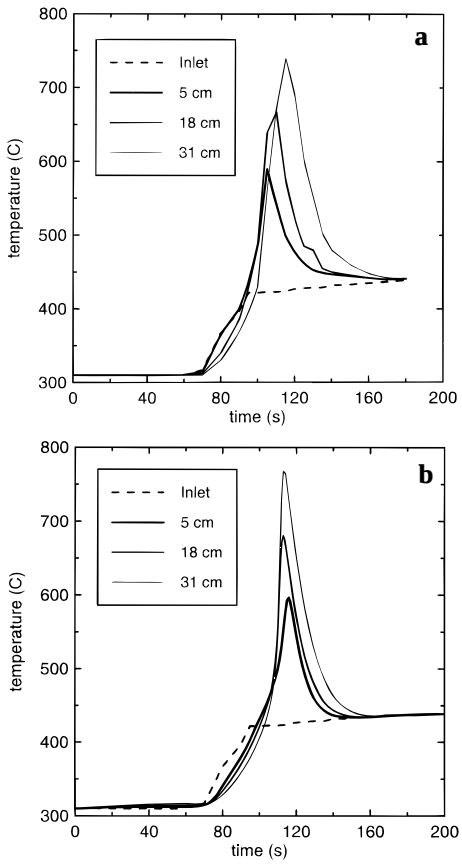

Figure 3. Temperatures inside the filter during high space velocity regeneration for a highly loaded filter (155 g of particulate mass): (a) measured (Tan et al., 1996); (b) computed.

deposit layer thickness. According to this figure, the soot is first oxidized near the entrance during the first 110 s. During this initial phase, the filter is in the preheating stage, where the prevailing phenomenon is convective heating of the channel. Toward the end of this phase, the developed soot thickness profile favors higher wall velocities near the channel inlet. The resulting higher residence times in the middle section favor higher reaction rates, leading to the profile shown at 115 s. Near the channel exit the soot remains

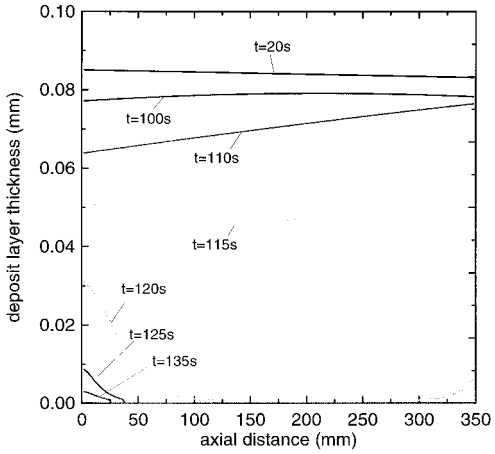

Figure 4. Computed profiles of the soot layer thickness along the filter channel during high space velocity regeneration for a highly loaded filter (155 g of particulate mass).

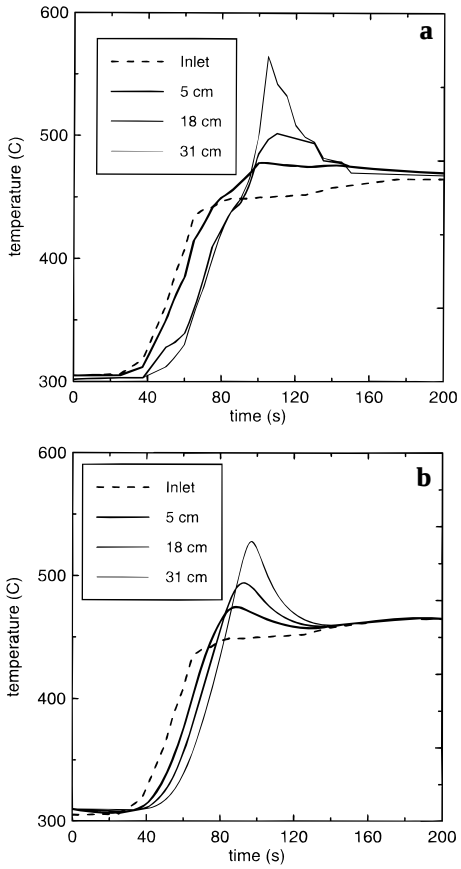

Figure 5. Temperatures inside the filter during high space velocity regeneration for a moderately loaded filter (63 g of particulate mass): (a) measured (Tan et al., 1996); (b) computed.

unoxidized. However, after $t = 115$ s, the resulting high temperatures and reaction rates favor the fast evolution of regeneration toward the channel exit. The only part of the soot layer that is not quickly depleted is the one adjacent to the inlet section. The filter is almost competely regenerated by $t = 135$ s.

Another example of the model capabilities is presented in the comparison of measured (Figure 5a) and computed (Figure 5b) evolution of a high space velocity regeneration with lower initial soot loading. The attained accuracy is remarkable if one takes into account the significant differences in temperature evolution in the different channels of this large diameter filter (Tan et al., 1996).

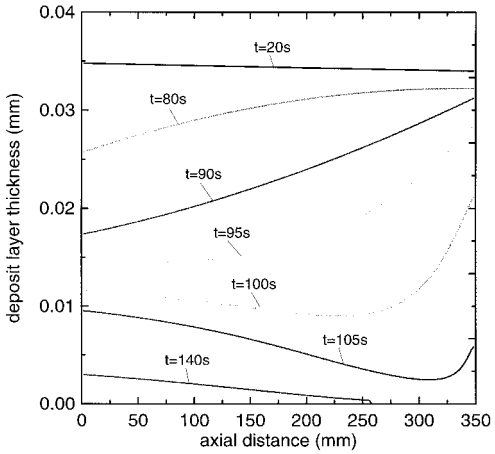

Figure 6. Computed profiles of the soot layer thickness along the filter channel during high space velocity regeneration for a moderately loaded filter (63 g of particulate mass).

A deeper insight in this regeneration may be gained by a closer inspection of the computed reaction propagation, presented in Figure 6. Similar to the previous example, the convective heating of the filter channels is the dominating phenomenon responsible for soot oxidation during the preheating stage (first 95 s). Due to the lower soot loading of the filter in this case, the evolution of the regeneration is smoother, exhibiting the same stages as in the previous case.

In order to demonstrate accuracy improvements stemming from the one-dimensional character of the present model, the results of comparative runs with the zero-dimensional model (Koltsakis and Stamatelos, 1996a) for the moderately loaded filter regeneration are given in Figure 7. Although the 0D model predicts the onset of regeneration about 10 s later, complete filter cleaning is observed earlier than the predictions of the 1D model (Figure 7a).

To explain the different behaviors of the two models, Figure 7b compares the filter exit temperatures computed by the two models, as well as the maximum filter temperature computed by the 1D model. Also shown are measured wall temperatures at 5 cm from the filter exit (at centerline). During the preheating stage, the computed filter exit temperatures by the two models are in good agreement. However, the 0D model cannot take into account convective heat-transfer effects in the channel which lead to a significant overheating of the frontal part of the filter. These higher temperatures near the filter inlet face are responsible for the onset of regeneration, which is predicted by the 1D model. The maximum filter exit temperature computed by the 1D model is higher than the maximum temperature computed by the 0D model. Obviously, the 1D model in this case gives more reliable results regarding the thermal loading of the filter, which is related to its durability.

Regeneration at Low Space Velocities. This is the second mode of regeneration encountered in practice. This second mode is frequently occurring in a filter system operating with catalytic additive doped fuel, during city driving with frequent vehicle braking. This regeneration mode is characterized by increased wall temperature levels that sometimes jeopardize filter endurance (uncontrolled regeneration). Due to the low flow rates, there occur significant one-dimensional effects in the propagation of the reaction. Study of low space velocity regeneration will be done in this paper, by use of the 1D model, based on experimental recordings according to a specific scenario presented in Figure

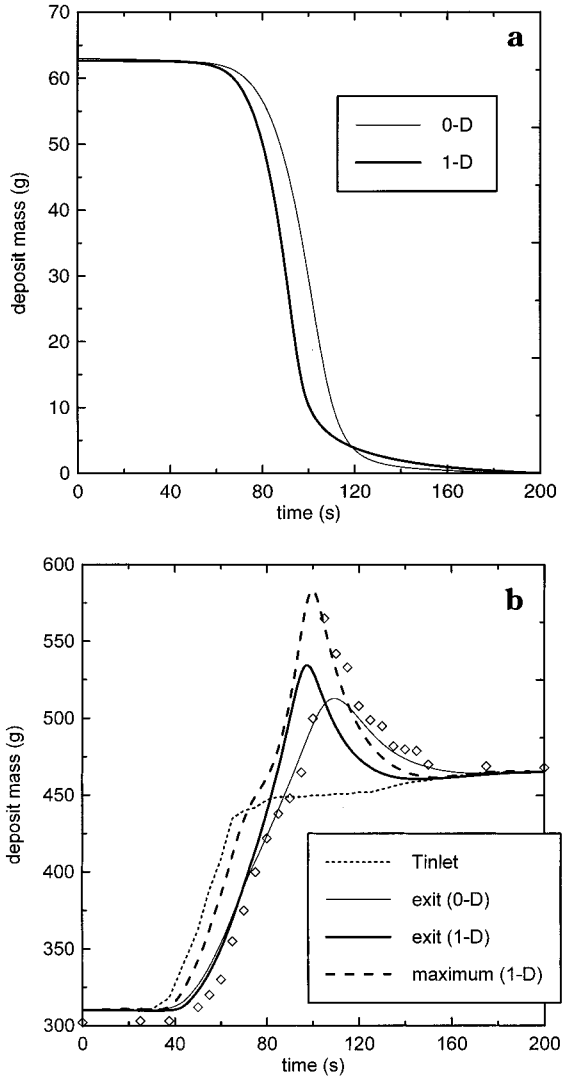

Figure 7. Comparison between the predictions of the zero-dimensional and the one-dimensional models during high space velocity regeneration for the moderately loaded filter (63 g of particulate mass). (a) Computed filter particulate loading. (b) Computed maximum and exit temperatures. Also shown, for comparison, are measured temperatures 5 cm from the filter exit (◇).

8. It should be noted here that, throughout the experiments with low space velocity 66 ppm of Lubrizol, a copper-based fuel additive was used. In order to carry out this computation, a respective doubling of the additive oxides concentration inside the soot layer (ξ) was used as input. This significant change in additive dosage is a good check for the fuel-additive activity submodel.

Figure 9a shows the recorded temporal evolution of temperatures at the three characteristic points along the filter axis, during a regeneration with a highly loaded filter, that led to filter failure. The highest temperature in this experiment (1183 °C) was not recorded along the filter axis but at a channel located half-way from the axis to the periphery. This regeneration is a quite demanding simulation case for the 1D model validation.

The results of applying the 1D model to the regeneration of Figure 9a are presented in Figure 9b. The model shows a good prediction ability, in regards to the onset of regeneration in different points along the axis. Also, prediction of regeneration at the middle point (18 cm from the inlet) is quite accurate. At 5 cm an about 100

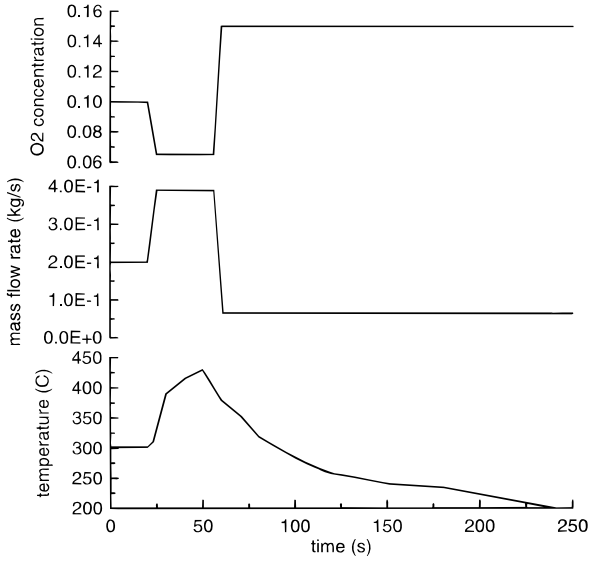

Figure 8. Low space velocity regeneration scenario employed in this study. Exhaust gas temperature at filter inlet, exhaust gas flow rate, and oxygen content as functions of time.

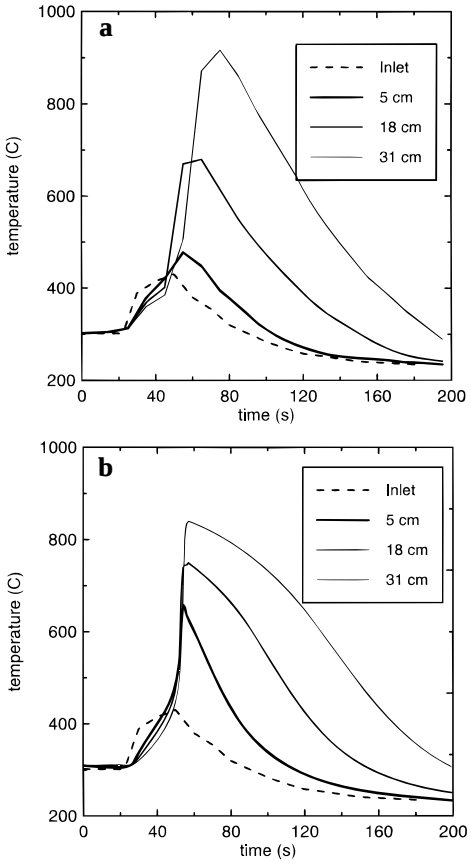

Figure 9. Temperatures inside the filter during low space velocity regeneration for a highly loaded filter (135 g of particulate mass): (a) measured (Tan et al., 1996); (b) computed.

°C higher temperature peak is predicted. On the contrary, the maximum temperature predicted at 31 cm from the inlet is about 100 °C lower than the measured one. Possible explanations for this deviation are investigated in the next section.

Figure 10 shows the computed temporal evolution of axial profiles of the deposit layer thickness. During the initial preheating stage (first 52 s) soot oxidation is observed near the filter inlet, where the prevailing temperatures are higher due to convective heating.

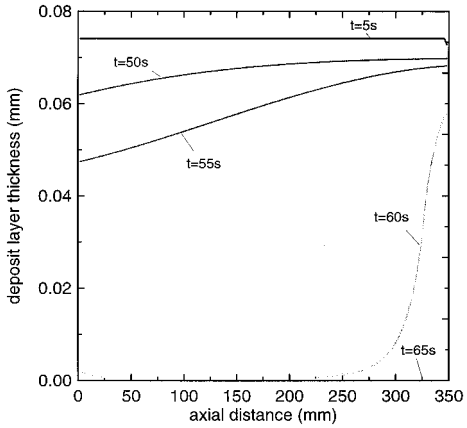

Figure 10. Computed profiles of the soot layer thickness along the filter channel during low space velocity regeneration for a highly loaded filter (135 g of particulate mass).

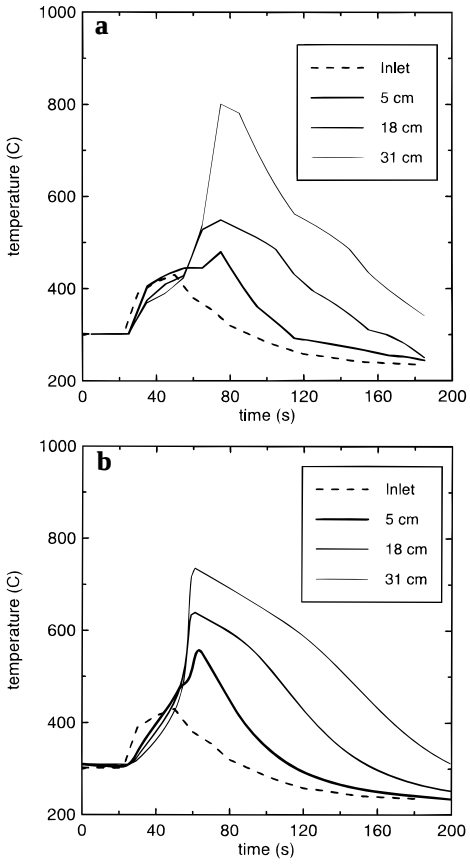

Figure 11. Temperatures inside the filter during low space velocity regeneration for a moderately loaded filter (107 g of particulate mass): (a) measured (Tan et al., 1996); (b) computed.

After shifting the engine operation point to idle, the lower flow rates and the higher oxygen content cause much higher reaction rates, leading to almost complete soot depletion for the first 25 cm from the inlet. At t = 65 s the regeneration is completed.

In order to further validate the model in low space velocity regeneration, the regeneration presented in Figure 11 was selected. This is a regeneration with lower soot loading (again, 66 ppm copper in the fuel consumed), which led to severe thermal loading of the filter, which, however, was not fatal. The combination of the two experiments would be a good test case for the capacity of the model to predict the risk level of different soot loadings regarding filter failure.

According to the computational results of Figure 11b,

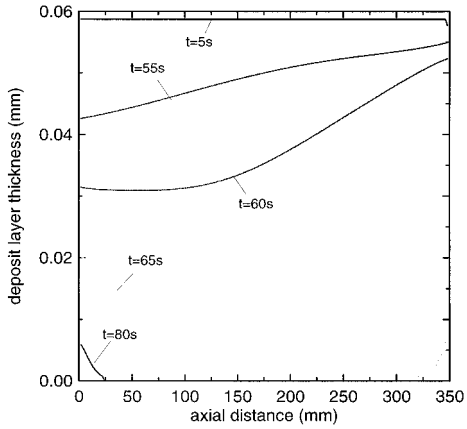

Figure 12. Computed profiles of the soot layer thickness and along the filter channel during low space velocity regeneration for a moderately loaded filter (107 g of particulate mass).

the model is again quite successful in predicting the onset of regeneration and the evolution of temperatures along the filter axis. Again, the temperature peak at 5 cm from the inlet is overestimated by about 50 °C. This obviously affects the evolution of the other two temperatures, so that the temperature peak at 31 cm from the inlet is underestimated by about 50 °C.

Although the temperature field evolution in the filter is analogous as in the previous case with the higher loading, examination of the soot deposit profiles as a function of time reveals some differences. As shown in Figure 12, the regeneration is also here initiated during the inlet temperature increase stage, lasting until t = 55 s. Due to the lower soot loading, the regeneration at the frontal part of the filter is not so intense to withstand the cooling from the feed gas, after t = 55 s. On the other hand, near the filter exit, the reaction is still slow until t = 60 s. At this stage, the more favorable regeneration conditions are met near the middle of the filter, leaving soot residuals near the inlet and the outlet of the filter. The filter is almost completely cleaned after t = 80 s.

The results of comparative runs with the zero-dimensional model for the moderately loaded filter regeneration at low space velocity are given in Figure 13. The 0D model predicts a delayed onset of regeneration by about 7 s, for the same reasons analyzed for Figure 7. Moreover, the filter wall temperature predicted by the 0D model is about 100 °C lower than the one predicted by the 1D model (a measure of the real filter wall temperature levels is given in Figure 13b by means of measured wall temperatures at a centerline point, 5 cm from the filter exit). It can be also noted here that the maximum temperature computed by the 1D model occurs near the filter exit, which is also what is measured in practice (Tan et al., 1996).

Beyond the 1D Approach. A good accuracy of the 1D model has been demonstrated in the prediction of temperatures along the filter axis, in the cases of high and low space velocity regeneration with different soot loadings. It should be recalled that, in order to demonstrate the model capabilities, we selected an already published experimental case study employing a copper-based fuel additive. This study comprises only full-scale regeneration experiments, which means that no detailed information on the reaction kinetics of the specific fuel additive was available.

Due to the high sensitivity of the catalytic regeneration process on the additive-assisted soot oxidation

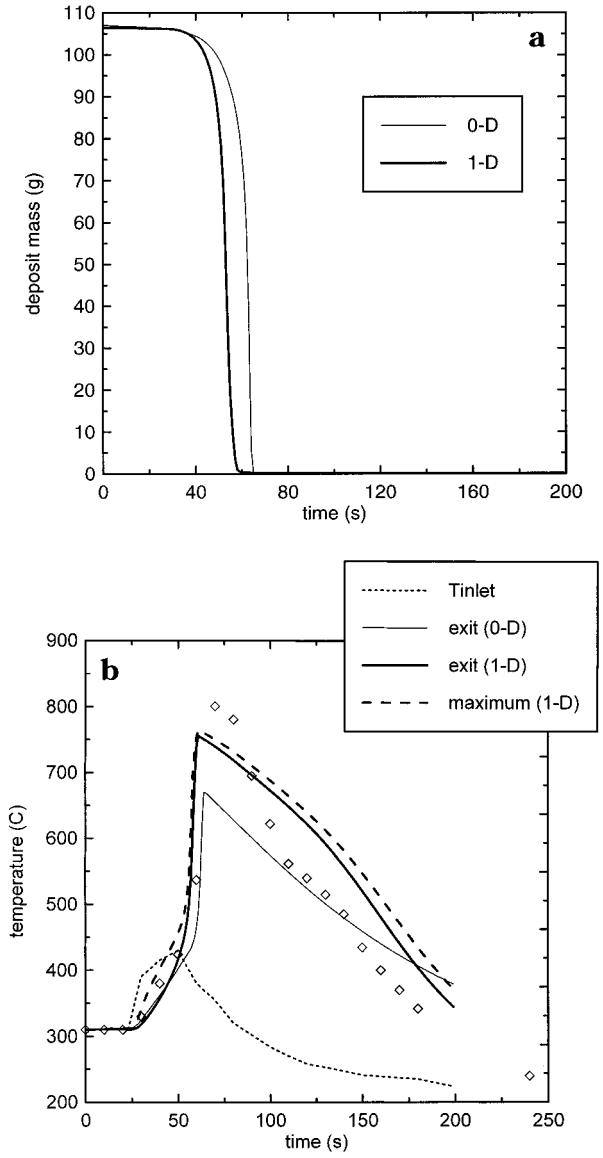

Figure 13. Comparison between the predictions of the zero-dimensional and the one-dimensional models during low space velocity regeneration for the moderately loaded filter (107 g of particulate mass). (a) Computed filter particulate loading. (b) Computed maximum and exit temperatures. Also shown, for comparison, are measured temperatures 5 cm from the filter exit (◇).

kinetics, the model could be effectively tuned to match real world behavior of the filter regeneration, based on these full-scale tests. Naturally, this first assessment of the kinetic, flow, and soot loading parameters is only preliminary. This is an obvious reason for the deviations between predictions and measurements, for example, in the temperature peak near the frontal part of the filter in the low space velocity regeneration. Apart from the reaction kinetics, additional degrees of freedom should be taken into account by a more sophisticated extended model of the process, in order to gain more accurate results. These degrees of freedom are related with the following phenomena:

Variations in the initial soot loading profile along the channel, produced by the soot deposition modes along the channel, result from the two-phase flow characteristics. This is a complex CFD problem that requires a significant experimental support. Such a study must take into account size distribution of the particulates in the exhaust and flow entrance effects. Previous

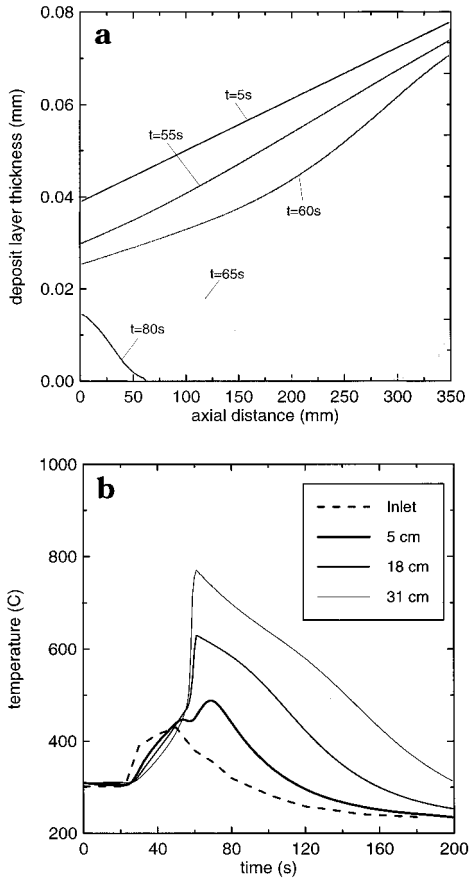

Figure 14. Computed low space velocity regeneration with a nonuniform initial soot layer thickness. All other parameters are the same as those of Figure 11: (a) profiles of soot layer thickness as a function of time; (b) filter temperatures at different positions.

experience, supported by preliminary calculations, indicates that a higher soot layer thickness is observed near the plugged channel end. The present model has the ability to predict the effect of this type of deposition nonuniformities, by suitably modifying the initial conditions.

An example is presented in Figure 14, where the same initial soot loading mass as in the case of Figure 11 was distributed with a linear nonuniformity starting, as shown in Figure 14a (t = 5 s). A comparison of the predicted temperatures in Figure 14b with the measured ones in Figure 11a shows a remarkable agreement. Thus, a possible explanation for the accuracy deviations of the computation of Figure 11b could be a soot loading nonuniformity.

Variations in the channel inlet velocity for different channels of the filter, due to flow maldistribution at the filter inlet face, are very well-known to occur in practice, due to frequent engine speed and load changes in city driving. Even in steady-state conditions, significant flow maldistribution has been recorded in a number of experiments with catalytic converters in gasoline cars (Bella et al., 1991). Exhaust flow maldistribution at the monolith inlet is induced by the catalyst upstream exhaust piping and diffuser layout, which is unfavorable for a uniform flow distribution.

Figure 15 is a prediction of the effect of differences in channel inlet velocity on the evolution of regeneration at a channel near the periphery of the monolith, compared to the baseline central channel. An initial 30% reduction in channnel velocity compared to the central channel is assumed during the full load part of

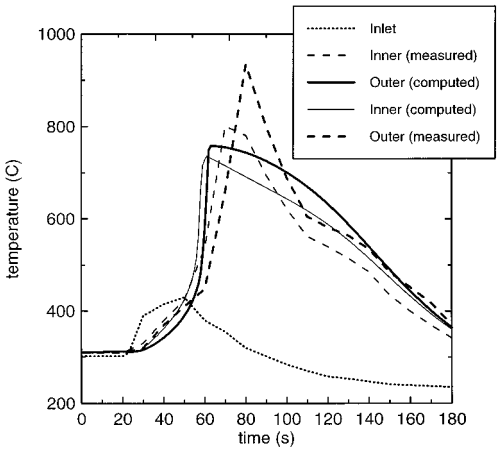

Figure 15. Computed and measured evolution of low space velocity regeneration in two different filter channels.

the scenario. However, after the onset of regeneration (peak temperature), no reduction is assumed in channel velocity during the engine idling part of the scenario (because the cleaning of the channel reduces its flow resistance in comparison to other, not yet clean, channels and increases respectively the flow velocity in the specific channel). In the same figure, a comparison is shown with the measured evolution of temperatures at the central and the more-close-to-periphery channel. It may be concluded that the lag in the regeneration of the external channel observed in the experimental results could be attributed to flow maldistribution effects.

Variations in the initial soot loading level and profile for the different channels are other important causes that may lead to significant differences in the evolution of soot oxidation and the resulting temporal evolution of temperatures. In the example of Figure 15 the peak temperature of 940 °C recorded at the external channel is significantly higher than the one predicted with the modified flow velocity. Based on previous research results (Koltsakis and Stamatelos, 1996a; Bissett and Shadman, 1983), the higher peak temperature must be attributed to a higher local soot loading.

Concluding Remarks

In response to the need for computational tools supporting the development of advanced diesel particulate filter systems, a mathematical model of the catalytic filter regeneration process has been developed and validated.

The present model, which is an extension of a previous zero-dimensional catalytic regeneration model, is capable of predicting the spatial propagation of the regeneration front and its dependence on reactor design, process conditions, and catalyst dosimetry.

In order to check the performance of the model in a variety of regeneration modes, an already published set of full-scale experimental results has been employed. The kinetics of the fuel-additive activity submodel were successfully assessed based on these results. This was confirmed by the quality and accuracy of predictions in quite different regeneration modes and fuel-additive concentrations.

The above-mentioned procedure led us to a better understanding of the propagation of the regeneration reaction along the filter axis, by observing, in addition to temperatures, also the temporal evolution of soot layer thickness profiles.

Possible explanations for the minor deviations of the model results from reality have been stated and discussed. Selected model runs were performed to assess the extents of the effects of inlet flow maldistribution, as well as nonuniform soot deposition (axially and radially). Significant experimental effort should be devoted to the better understanding of these effects.

Nomenclature

C_{pg} = specific heat capacity of exhaust gas, 1090 J/(kg K)
C_{p1} = specific heat capacity of soot deposit, 1510 J/(kg K)
C_{p2} = specific heat capacity of ceramic wall, 1120 J/(kg K)
D = hydraulic diameter of channel
Da = Damkoehler number
E = apparent activation energy of soot oxidation, 150×10^3 J/mol
E_{ox} = activation energy for metal additive oxidation, 107×10^3 J/mol
E_{red} = activation energy for metal additive reduction, 107×10^3 J/mol
h = heat convection coefficient, W/(m^2 K)
H_{react} = reaction heat release, W/m^2
H_{cond} = conductive heat flux, W/m^2
ΔH = "combined" reaction enthalpy of soot oxidation, J/mol
$\Delta H_{(i)}$ = specific heat of CO_2 formation, 3.61×10^5 J/mol
$\Delta H_{(ii)}$ = specific heat of CO formation, 0.90×10^5 J/mol
k_1 = rate coefficient for the soot combustion reaction, m/s
k = collisions frequency factor, 1.0 m/(s K)
k_{ox} = rate coefficient for fuel additive oxidation
k_p = permeability of particulate deposit layer, 1.1×10^{-14} m^2
k_{red} = rate coefficient for fuel additive reduction
k_s = permeability of ceramic substrate, 1.54×10^{-13} m^2
M_{O_2} = molecular weight of exhaust gas, 29×10^{-3} kg/mol
M_c = atomic weight of deposit, 12×10^{-3} kg/mol
p = exhaust gas pressure, Pa
R = gas constant, 8.31 m^3 Pa/(mol K)
S_p = specific area of deposit layer, 5.5×10^7 m^{-1}
T = temperature, K
t = time, s
v = velocity, m/s
w = thickness of the deposit layer, m
w_s = channel wall thickness, m
x = distance, m
y = oxygen concentration of the exhaust gas (mole fraction)
z = axial distance, m

Greek Letters

α = index for the completeness of thermal soot oxidation
α_1 = constant in channel pressure drop correlation, 28.45
ΔP = trap backpressure, Pa
λ_p = particulate thermal conductivity, 2.1 W/(m K)
λ_s = substrate thermal conductivity, 0.85 W/(m K)
μ = exhaust gas viscosity
ξ = defined in eq 11
ρ = exhaust gas density, kg/m^3
ρ_p = bulk density of the deposit layer, 140 kg/m^3
ρ_s = bulk density of porous ceramic, 1400 kg/m^3
ψ = defined in eq 12

Subscripts

b = initial condition
cat = catalytic
i = 1, 2 = inlet, outlet channel
p = particulate layer
s = substrate

w = wall

Literature Cited

Ahlstroem, A. F.; Odenbrand, C. U. I. *Appl. Catal.* **1990**, *60*, 143−156.

Aoki, H.; Asano, A.; Kurazono, K.; Kobashi, K.; Sami, H. Numerical Simulation Model for the Regeneration Process of a Wall-Flow Monolith Diesel Particulate Filter. SAE Paper 930364; SAE: Warrendale, PA, 1993.

Bella, G.; Rocco, V.; Maggiore, M. A Study of Inlet Flow Distortion Effects on Automotive Catalytic Converters. *J. Eng. Gas Turbines Power*, **1991**, *113*, July, 419−426.

Bissett, E.; Shadman, F. Thermal Regeneration of Diesel-Particulate Monolithic Filters. *AlChE J.* **1985**, *31* (5), May, 753.

Cotton, D. H.; Friswell, N. J.; Jenkins, D. R. *Combust. Flame* **1971**, *17*, 87−98.

De Soete, G. Combustion Catalytique des Suies Formees en Phase Gazeuse a Partir de Diesel-oils. Institut Francais du Petrole Techniques d'applications Energetiques, Report IFP No. 35378, June 1987.

Hoffmann, U.; Ma, J. Study on Regeneration of Diesel Particulate Filter Using a Laboratory Reactor. *Chem. Eng. Technol.* **1990**, *13*, 251−258.

Hoffmann, U.; Rieckmann T.; Ma, J. Kinetic Study and Modelling of Diesel Particulate Filter Regeneration. *Chem. Eng. Sci.* **1991**, *44*.

Johnson, J.; Bagley, S. T.; Gratz, L.; Leddy, D. A Review of Diesel Particulate Control Technology and Emissions Effects−1992 Horning Memorial Award Lecture. SAE paper 940233; SAE: Warrendale, PA, 1994.

Koltsakis, G. C.; Stamatelos, A. M. Modeling Catalytic Regeneration of Wall-Flow Particulate Filters. *Ind. Eng. Chem. Res.* **1996a**, *35*, 2−13.

Koltsakis, G. C.; Stamatelos, A. M. Modeling Thermal Regeneration of Wall-Flow Diesel Particulate Traps. *AIChE J.* **1996b**, *42* (6), June.

Lepperhoff, G.; Kroon, G. *Abgasnachbehandlung I* (Abschlussbericht); FVV-Heft 352, 1984.

Lepperhoff, G.; Lueders, H.; Barthe, P.; Lemaire, J. Quasi-Continuous Particle Trap Regeneration by Cerium-Additives. SAE paper 950369; SAE: Warrendale, PA, 1995.

Lox, E. S.; Engler, B. H.; Koberstein, E. Diesel Emission Control. In *Catalysis and Automotive Pollution Control II*; Crucq, A., Ed.; Elsevier Science Publishers B.V.: Amsterdam, The Netherlands, 1991.

McCabe, R. W.; Sinkevitch, R. M. Oxidation of Diesel Particulates by Catalyzed Wall-Flow Monolith Filters. SAE paper 870009; SAE: Warrendale, PA, 1987.

McKee, D. W. The Catalyzed Gasification Reactions of Carbon. *Chem. Phys. Carbon* **1981**, *16*, 183−199.

Pattas, K. N.; Michalopoulou, C. C. Catalytic Activity in the Regeneration of the Ceramic Diesel Particulate Trap. SAE paper 920362; SAE: Warrendale, PA, 1992.

Pattas, K. N.; Patsatzis, N. A.; Michalopoulou, C. C.; Stamatelos, A. M.; Kikidis, P. S.; Samaras, Z. C.; Sowul, H. Ceramic Trap Regeneration Rate Control through Bypass Technique. SAE paper 880004; SAE: Warrendale, PA, 1988.

Pattas, K. N.; Samaras, Z. C.; Patsatzis, N. A.; Michalopoulou, C. C.; Zogou, O.; Stamatelos, A. M.; Barkis, M. On-Road Experience with Trap Oxidiser Systems Installed on Urban Buses. SAE paper 900109; SAE: Warrendale, PA, 1990.

Pattas, K. N.; Stamatelos, A. M.; Koltsakis, G. C.; Kandylas, I. P.; Mustel, W. Computer Aided Engineering in the Design of Catalytically Assisted Trap Systems. SAE paper 970472; SAE: Warrendale, PA, 1997.

Sorenson, S.; Hoj, J.; Stobbe, P. Flow Characteristics of SiC Diesel Particulate Filter Materials. SAE paper 940236; SAE: Warrendale, PA, 1994.

Tan, J. C.; Opris, C. N.; Baumgard, K. J.; Johnson, J. H. A Study of the Regeneration Process in Diesel Particulate Traps Using a Copper Fuel Additive. SAE paper 960136; SAE: Warrendale, PA, 1996.

Vuk, C. T.; Jones, M. A.; Johnson, J. H. The measurement and analysis of the physical character of diesel particulate emissions. SAE paper 760131; SAE: Warrendale, PA, 1976.

Wiedemann, B.; Doerges, U.; Engeler, W.; Poettner, B. Regeneration of Particulate Filters at Low Temperatures. SAE paper 830086; SAE: Warrendale, PA, 1983.

Yuan, S.; Meriaudeau, P.; Perrichon, V. *Appl. Catal. B* **1994**, *3*, 319−333.

Zelenka, P.; Cartellieri, W.; Herzog, P. Worldwide diesel emission standards, current experiences and future needs. *Appl. Catal. B* **1996**, *10* 3−28.

Received for review January 31, 1997
Revised manuscript received June 16, 1997
Accepted June 16, 1997[⊗]

IE970095M

[⊗] Abstract published in *Advance ACS Abstracts,* August 15, 1997.